

PhotoD: LSST photometric distances out to 100 kpc.

LOVRO PALAVERSA ¹, ŽELJKO IVEZIĆ ², AND KARLO MRAKOVČIĆ ³

¹*Ruder Bošković Institute, Bijenička cesta 54, 10000 Zagreb, Croatia*

²*Department of Astronomy, University of Washington, Box 351580, Seattle, WA 98195, USA*

³*Faculty of Physics, University of Rijeka, Radmile Matejčić 2, 51000 Rijeka, Croatia*

ABSTRACT

Abstract here, mind the 250 word limit.

Keywords: Distance measure (395) — Interstellar extinction (841) — Photometry (1234) — Stellar distance (1595) — Two-color diagrams (1724)

1. INTRODUCTION

Thanks to the *Vera C. Rubin* observatory's *Legacy Survey of Space and Time* (LSST), for the first time in history, an astronomical catalog will contain more Milky Way stars than there are living people on Earth – of the order 10-20 billion, depending on model assumptions. In order to map the Milky Way in three dimensions, distances to these stars must be accurately estimated. In this paper we describe a method that will deliver LSST-based stellar distance estimations complementary to *Gaia*'s state-of-the-art trigonometric parallaxes and reach about 10 times further, to approximately 100 kpc. These results will be transformative for the studies of the Milky Way in general, and the stellar and the dark matter halo in particular as never before was there a survey that simultaneously observed roughly two thirds of the sky, to the co-added depth of $r \approx 26$ mag.

A bit about the importance of the distance estimation in the MW, dust implications (for extragalactic science too).

There are a variety of astronomical methods to estimate distances to stars, ranging from direct geometric (trigonometric) methods for nearby stars to indirect methods based on astrophysics for more distant stars.

Mention Bailer-Jones et al. (2021), Gordon et al. (2016), Green et al. (2014, 2015, 2019), Jurić et al. (2008) and Lallement et al. (2014), Queiroz et al. (2018).

Layout of the paper is...

2. METHOD

The photometric distance estimation method (hereafter **photoD**) is conceptually quite simple and relies on the strong correlations between the stellar colors and spectral energy distributions (SED) for dominant stellar populations. The SEDs, and consequently colors, are determined by the effective temperature (T_{eff}), the surface gravity (usually denoted as $\log(g)$), and the metallicity ($[M/H]$), or alternatively, by the absolute magnitude in band b (M_b), $[M/H]$ and age.

The distributions that describe these correlations are obtained either from models or from observations. For example, the distribution of stellar SEDs in the color-color diagram in the middle and left panels of Figure 1 provide key insights in stellar evolution and classification of different stellar populations such as main-sequence stars, giant stars, white dwarf stars, a majority of unresolved binary stars and even extragalactic objects. Analogous distributions are responsible for the abundant structure seen in the Hertzsprung-Russell diagram (HRD).

Metallicity is an important factor in these correlations, as it has a strong effect on the luminosity of the stars. This is reflected in the width of the main stellar loci of the two-color diagrams (middle and right hand panels in Figure 1 and the color-absolute magnitude diagrams (CAMD) in Figure 2. The best photometric estimators of metallicity are colors whose shorter-wavelength component includes the metal absorption bands at near-UV wavelengths, short of Balmer break ($300 \lesssim \lambda$ [nm] $\lesssim 400$). Therefore, the LSST has a comparative advantage over the surveys lacking u -band measurements, and could provide accurate distances within the range of 5-10%. **A plot of model spectra, fixed, $\log(g)$ and T_{eff} , several different metallicities?**

Extinction is another major source of systematic errors in the process of luminosity and distance determination. The fact that the extinction vector is nearly parallel to the main stellar locus in the two-color diagrams gives rise to degeneracies that complicate the determination of the stellar type. An example is displayed in Figure 3, where in the left panel any of the different star types designated as 1,2 and 3 can have the same observed colors as the star marked as "Obs". This degeneracy is a result of the combination of colors chosen for the two-color diagram and depends on the position on the stellar locus and the adopted extinction curve parametrized by a single parameter R_V

$$R_V = \frac{A_V}{E(B-V)}, \quad (1)$$

where A_V stands for extinction in V -band and $E(B-V)$ is the color excess. This relationship can be extended to an arbitrary photometric bandpass λ :

$$A_\lambda = C_\lambda(R_V)A_r, \quad (2)$$

with A_r designating extinction in r -band and $C_\lambda(R_V)$ describing the shape of the extinction curve. The degeneracy from the left panel in Figure 3 can be broken if several different colors are used, particularly those towards the infrared. There the stellar locus is not as kinked and the extinction vector is not parallel to it. A possible example is shown in the right-hand panel of the Fig. 3, where $r-i$ and $i-z$ colors are used, and assuming a fixed extinction law a unique solution for the extinction is possible.

Explain the choice of RV .

Another important degeneracy arises from the fact that even for a fixed T_{eff} and $[Fe/H]$, the $\log(g)$ and thus the luminosity are not uniquely determined by the colors: a degeneracy may exist between the giant branch and the main sequence as the colors constructed from $ugrizy$ bands are not sensitive to $\log(g)$. We treat this issue by adopting a prior based on bins in apparent magnitude.

We adopt a Bayesian framework in which we simultaneously fit for M_b , $[Fe/H]$ and A_r , assuming a fixed RV value of 3.1¹ The posterior for each individual star with LSST photometry is then given as:

$$P(M_b, [Fe/H], A_r | \vec{c}) = \frac{P(\vec{c} | M_b, [Fe/H], A_r) P(M_b, [Fe/H], A_r)}{P(\vec{c})} \quad (3)$$

with \vec{c} standing for the vector of input colors ($u-g$, $g-r$ and so on). The log-likelihood is given by:

$$\ln(\mathcal{L}) = C - \frac{1}{2} \sum_{i=1}^N \left(\frac{c_i^{\text{obs}} - c_i^{\text{mod}}}{\sigma_i} \right)^2 \quad (4)$$

where c_i^{obs} are the observed colors and c_i^{mod} model colors. The values of model colors and the priors are extracted from TRILEGAL (Dal Tio et al. (2022)). In order to extract the priors (i.e. prior maps), we divide TRILEGAL data in healpix bins, and further subdivide them in one-magnitude wide bins in apparent magnitude. The latter subdivision is helpful in breaking the degeneracies between the giant and dwarf stars, as in-

¹ In principle RV could be also fitted for.

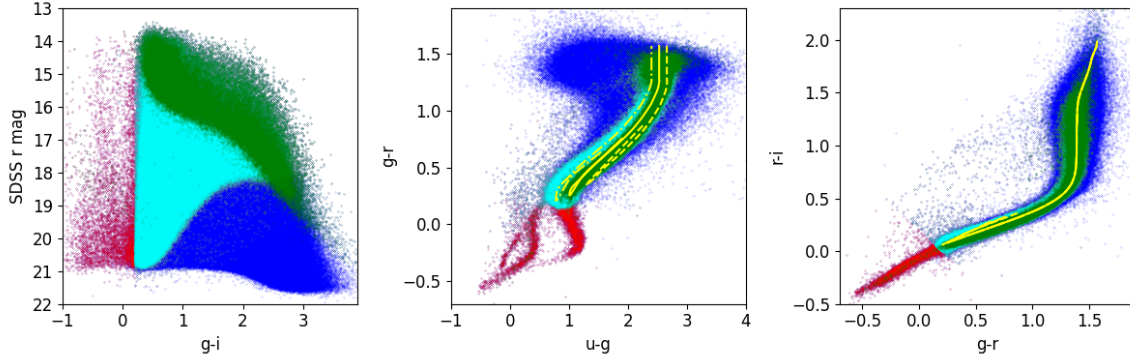


Figure 1. The blue dots in the left panel show color-magnitude diagram for 841,000 stars from the SDSS Stripe 82 Standard Star Catalog that have Gaia matches within 0.15 arcsec (after correcting for proper motion using Gaia measurements). A subset of 415,000 stars with $r < 22$ and $u < 22$ are shown as red dots, and 409,000 of those that also have $0.2 < g - i < 3.5$ are shown as cyan dots. Finally, 63,000 stars that have signal-to-noise ratio for Gaia’s parallax measurements of at least 20 are shown as green dots. The same color scheme is used in other two panels. The three yellow lines in the middle panel show stellar locus parametrization used by Green et al. (2014) for three values of metallicity (left to right): $[Fe/H] = -2.0, -1.0, 0.0$. In the right panel, the impact of metallicity on color-color tracks is negligible and all three are indistinguishable from each other.

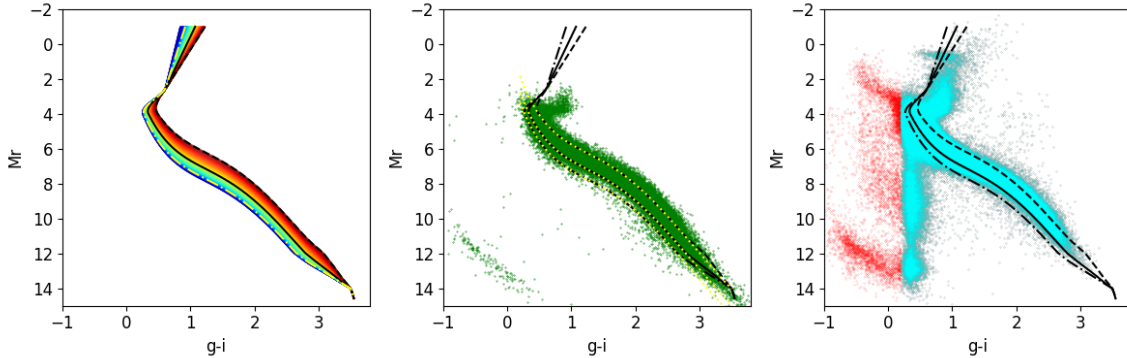


Figure 2. The left panel shows the absolute magnitude vs. color parametrization for main sequence and red giant stars. The symbols are color-coded by metallicity, ranging from $[Fe/H] = -2.5$ to 0.0 (blue to red). The three lines correspond to three values of metallicity: $[Fe/H] = -2.0, -1.0, 0.0$ (dot-dashed, solid and dashed, respectively). The middle panel shows a sample of 63,000 stars that have signal-to-noise ratio for Gaia’s parallax measurements of at least 20 (white dwarfs can be seen in the lower left corner). The dot-dashed, solid and dashed black lines are the same as in the left panel. For comparison, the dotted lines were computed using eqs. A2 and A7 from Ivezić et al. (2008). The right panel shows a sample of 415,000 stars with $r < 22$ and $u < 22$ as red dots, and 409,000 of those that also have $0.2 < g - i < 3.5$ as cyan dots. Their absolute magnitudes were computed using the so-called “photo-geometric” distances from Bailer-Jones et al. (2021). The dot-dashed, solid and dashed black lines are the same as in the left and middle panels. About 10,000 outliers seen at $g - i = 0.4$ and $Mr > 7$ are predominantly found at the faint end ($r > 20$).

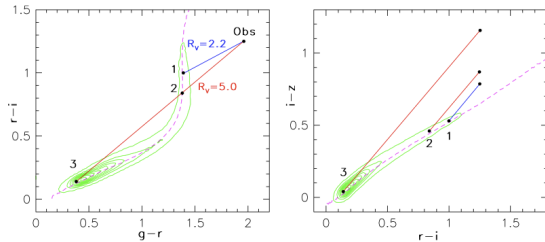


Figure 3. Add caption.

126 trinsically luminous stars become strongly disfavored at
127 faint magnitudes².

128 Add plots describing the method, and go through one
129 example like in Željko’s slides.

130 Our method is basically brute-force fitting with some
131 intelligent tricks leveraged to obtain faster execution

² In other words, an apparently faint giant star would imply a very large distance. For example a moderately bright giant star with $M_r = 0$ mag and $r = 22$ mag would imply a distance modulus of 22 mag, or distance of approximately 251 kpc.

132 that will be required for 10B LSST stars. We use
 133 [Schlegel et al. \(1998\)](#) (SFD98) maps in order to limit the
 134 range of the extinction. This is usually a valid assump-
 135 tion because the SFD98 maps provide *total* extinction
 136 along a line of sight. Our fitting procedure is also exe-
 137 cuted on an adaptive grid, a coarse search over the pa-
 138 rameter space is performed first in order to establish the
 139 layout of the manifold. However, care is taken that any
 140 possible local minima are not missed by appropriately
 141 adjusting the step size [how?](#). The located maxima are
 142 then explored with a smaller step size ([adjusted how?](#)).

143 In addition to the approach described here, we also
 144 tested Markov Chain Monte Carlo and neural net-
 145 work approaches that will be/are described in forthcom-
 146 ing/published papers.

147 [Advantages & disadvantages of the model-based and](#)
 148 [empirical approaches, how model based approaches can](#)
 149 [be improved by adding empirical information for specific](#)
 150 [cases.](#)

151 [Gordon et al. \(2016\)](#) na BEAST webu imaju zgodne
 152 diagrame; možda bi i mi mogli nešto tog tipa napraviti,
 153 bar za draft, primjer

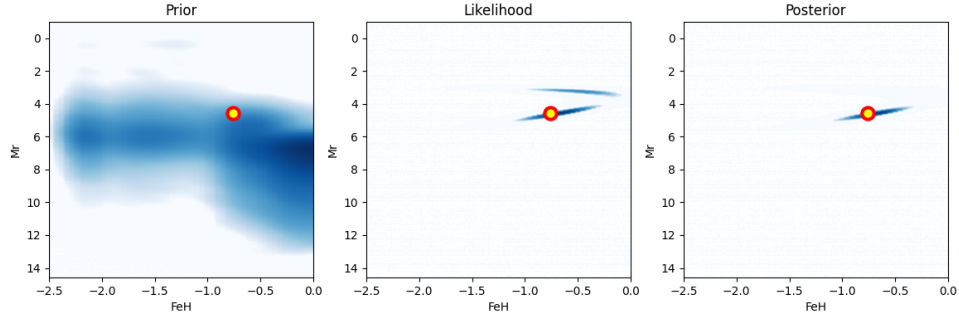


Figure 4. Write caption: prior, likelihood, posterior maps

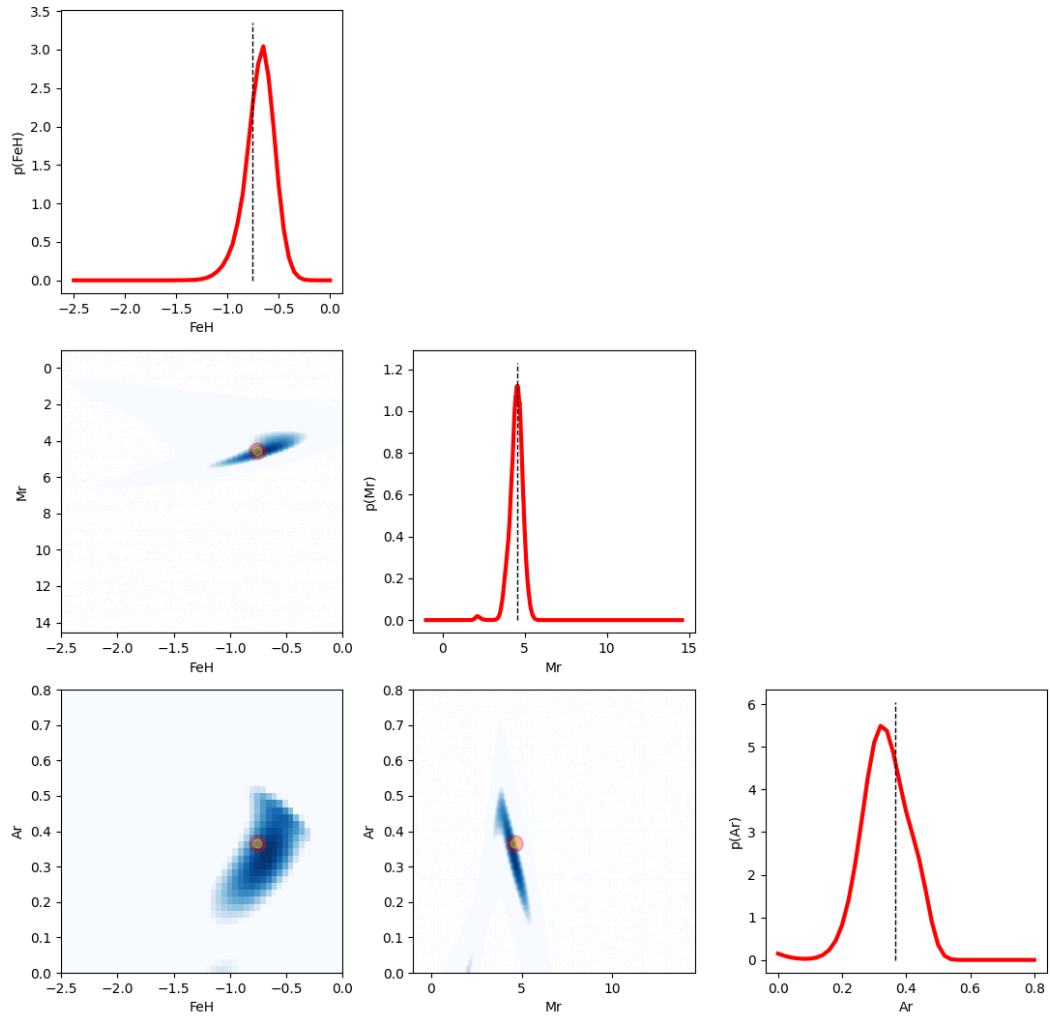


Figure 5. Write caption: 2-param covariances and marginal distributions

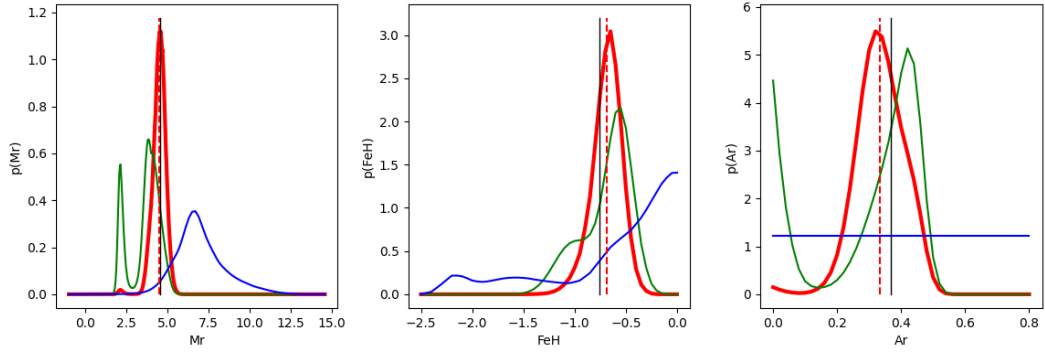


Figure 6. Write caption: prior, likelihood, posterior marginal distributions

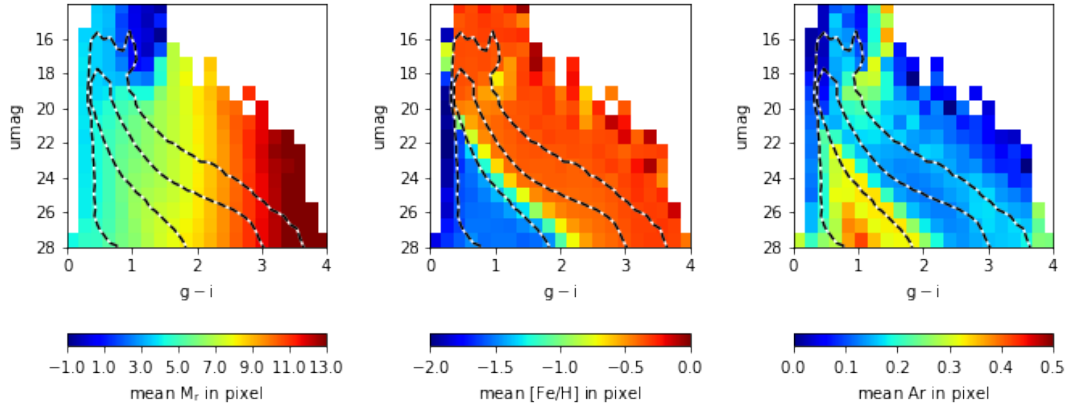


Figure 7. Write caption: TRILEGAL mean values of input model params in $umag$ vs. $g-i$

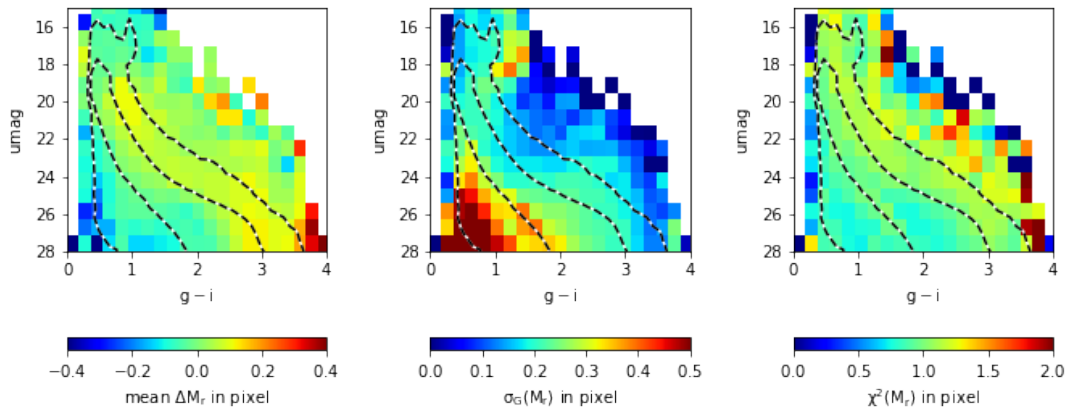


Figure 8. Write caption: performance for M_r vs. true M_r and FeH

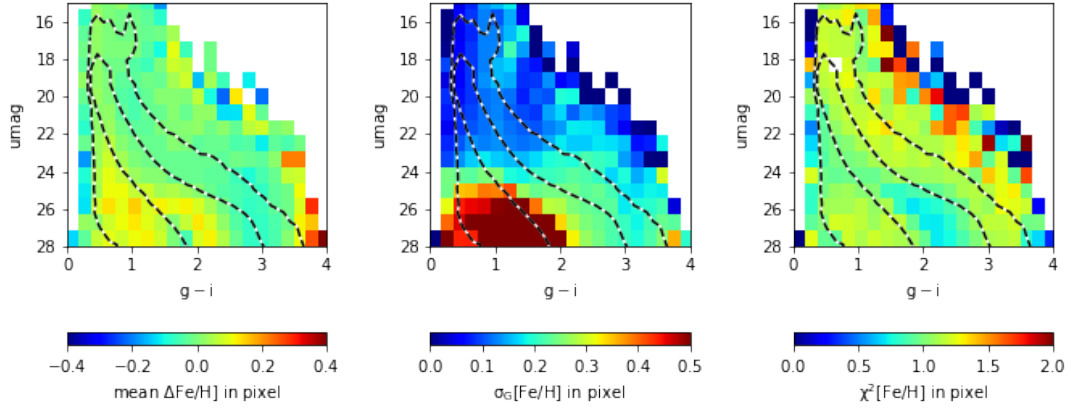


Figure 9. Write caption: performance for FeH vs. true Mr and FeH

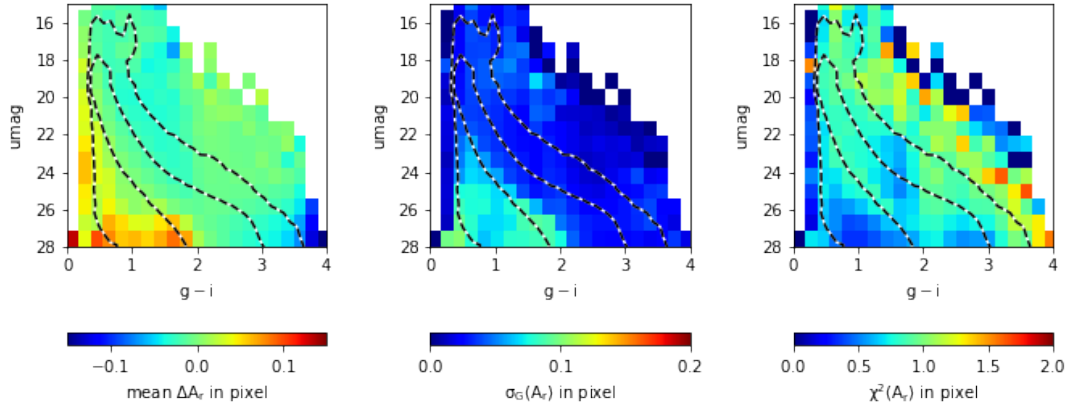


Figure 10. Write caption: performance for Ar vs. true Mr and FeH

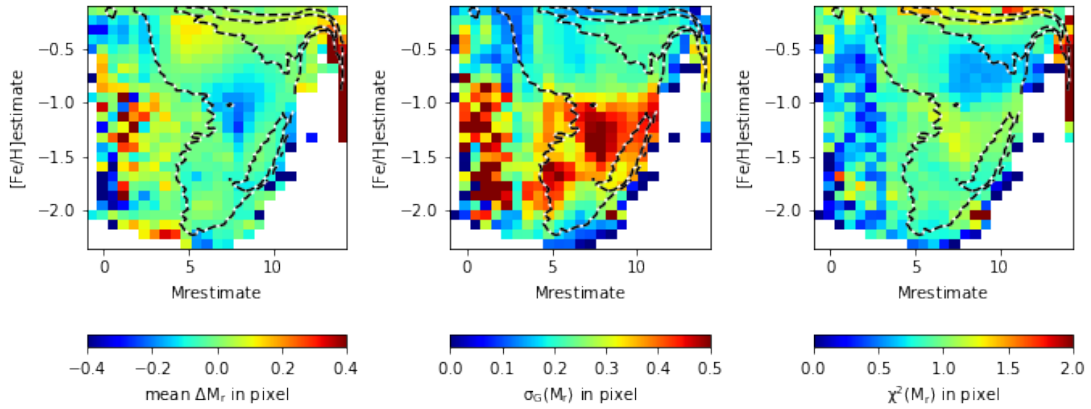


Figure 11. Write caption: performance for Mr vs. estimated Mr and FeH

APPENDIX

REFERENCES

- 155 Bailer-Jones, C. A. L., Rybizki, J., Fouesneau, M.,
 156 Demleitner, M., & Andrae, R. 2021, *AJ*, 161, 147,
 157 doi: [10.3847/1538-3881/abd806](https://doi.org/10.3847/1538-3881/abd806)
- 158 Dal Tio, P., Pastorelli, G., Mazzi, A., et al. 2022, *The*
 159 *Astrophysical Journal Supplement Series*, 262, 22,
 160 doi: [10.3847/1538-4365/ac7be6](https://doi.org/10.3847/1538-4365/ac7be6)
- 161 Gordon, K. D., Fouesneau, M., Arab, H., et al. 2016, *The*
 162 *Astrophysical Journal*, 826, 104,
 163 doi: [10.3847/0004-637X/826/2/104](https://doi.org/10.3847/0004-637X/826/2/104)
- 164 Green, G. M., Schlafly, E., Zucker, C., Speagle, J. S., &
 165 Finkbeiner, D. 2019, *The Astrophysical Journal*, 887, 93,
 166 doi: [10.3847/1538-4357/ab5362](https://doi.org/10.3847/1538-4357/ab5362)
- 167 Green, G. M., Schlafly, E. F., Finkbeiner, D. P., et al. 2014,
 168 *ApJ*, 783, 114, doi: [10.1088/0004-637X/783/2/114](https://doi.org/10.1088/0004-637X/783/2/114)
- 169 —. 2015, *ApJ*, 810, 25, doi: [10.1088/0004-637X/810/1/25](https://doi.org/10.1088/0004-637X/810/1/25)
- 170 Jurić, M., Ivezić, Ž., Brooks, A., et al. 2008, *The*
 171 *Astrophysical Journal*, 673, 864, doi: [10.1086/523619](https://doi.org/10.1086/523619)
- 172 Lallement, R., Vergely, J.-L., Valette, B., et al. 2014, *A&A*,
 173 561, A91, doi: [10.1051/0004-6361/201322032](https://doi.org/10.1051/0004-6361/201322032)
- 174 Queiroz, A. B. A., Anders, F., Santiago, B. X., et al. 2018,
 175 *Monthly Notices of the Royal Astronomical Society*, 476,
 176 2556, doi: [10.1093/mnras/sty330](https://doi.org/10.1093/mnras/sty330)
- 177 Schlegel, D. J., Finkbeiner, D. P., & Davis, M. 1998, *The*
 178 *Astrophysical Journal*, 500, 525, doi: [10.1086/305772](https://doi.org/10.1086/305772)